YU ISSN 0015—3206
FZKAAA 20 (4) 463 (1988)

TRANSITION TO OPTICAL TURBULENCE IN PHASE CONJUGATE RESONATORS

MILIVOJ R. BELIĆ

Institute of Physics, P. O. Box 57, 11001 Belgrade, Yugoslavia and Max-Planck-Institute für Quantenoptik, D-8046 Garching, Federal Republic of Germany

G. REINER

Dornier System GmbH, D-7990 Friedrichshafen, Federal Republic of Germany,

and

P. MEYSTRE

Optical Sciences Center, University of Arizona, Tucson, Az 85723, U. S. A.

Received 15 November 1988

UDC 535.374

Original scientific paper

Possible routes to optical turbulent state in a nonlinear phase conjugate resonator are investigated. Nonlinear dynamics of intracavity modes is followed by solving paraxial wave equation inside resonator using fast Fourier transform techniques, and a map relation. One transverse dimension is specifically included, and more than one control parameters are varied in our numerical experiments. It is found that the paths to chaos in this infinitely dimensional dissipative system include Feigenbaum period doubling, intermittency, and a Ruelle-Takens-Newhouse scenario. Other interesting phenomena are observed, such as inverse bifurcations, interior crises, and coexisting attractors. We compare and contrast our infinite dimensional optical system with its 2D approximation, treated by symbolic dynamical methods, and with other infinite systems, in particular with low aspect fluid flows, and with the Mackey-Glass and Ikeda time-delay models.

1. Introduction

This paper is dedicated to the memory of Professor Aleksandar Milojević, whose interest in lasers and nonlinear dynamical systems was well known and

appreciated. It seems, therefore, appropriate to present here an account on the transition to optical turbulence[1] in a phase conjugate resonator (PCR)[2]. In such a resonator one mirror is capable of conjugating the phase of the oncoming signal, i. e. in reversing the propagation of any incoming optical wavefront. PCR's with or without amplification are interesting because they can reduce or cancel distorsions or phase abberations in the cavity[2,3].

We say »optical turbulence« and not simply »chaos« because we include spatial effects in our dynamical analysis. Inclusion of the transverse effects is found to profoundly affect the nature of the transition. It increases the dimension of the system from two in the plane-wave model to infinitely many, and changes the transition from a period doubling Feigenbaum scenario to a Ruelle-Takens-Newhouse (RTN) scenario of few bifurcations of a limit cycle. In this respect our investigation parallels that of Le Berre et al.[4], where similarly a 2D adiabatic model of a NL ring cavity is contrasted with the time-delayed ∞D Ikeda model[5] of the same cavity.

NL optical systems are lately becoming of premier interest in studies of the onset of chaos[6]. They provide many interesting and convenient examples of chaotic behaviour: interesting because of the richness of phenomena observed[1,7], and convenient because they allow relatively simple modelling and experimentation (as compared, for example to fluid systems).

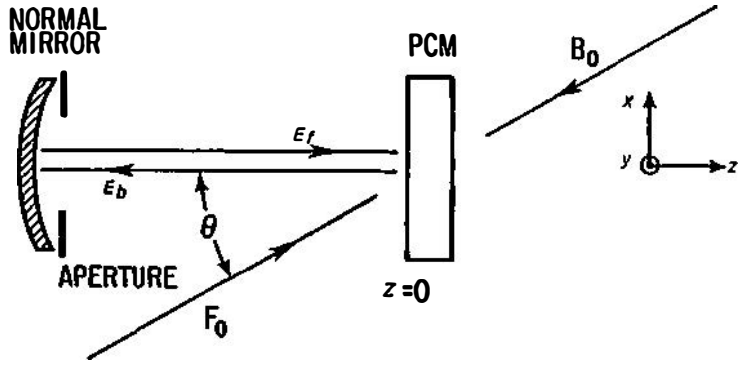

Fig. 1. Four-Wave Mixing PCR geometry used in the text. It allows scattered light at an angle Θ to be reflected back into the resonator.

The model considered by us is presented in Fig. 1. It is a PCR in which the phase conjugate mirror (PCM) consists of a Kerr-type medium operating in the Raman-Nath regime[8]. The normal mirror is positioned so as to return the first-order scattered light at an angle Θ back into the resonator. An aperture is placed in front of the mirror, whose width u will be one of the control parameters in the problem. The other control parameter will be the intensity of the laser pumps F_0 and B_0 pumping the Kerr-medium. We will follow the dynamics of intracavity modes by solving paraxial wave equation for the forward and the backward propagating fields E_f and E_b inside cavity. This is accomplished by different means, depending on whether we consider the plane wave 2D approximation or the full ∞D problem.

The PCR model described here has been investigated by us in a number of publications[9,10], and various aspects of its dynamical behaviour have already been presented. Here we continue our investigation by conducting a more detailed symbolic analysis of the 2D model, and by throwing more light onto the behaviour of the complete system when more than one control parameters are varied. Thus there are two aspects of the problem to be examined and clarified in this paper: the contrast between the 2D plane wave and the ∞D transverse model, and the changes within the ∞D model when more than one parameter is varied. In addition, our ∞D model will be compared with other infinite systems, notably with the Mackey-Glass (MG) time-delayed equation as analysed by Farmer[11], and instantaneous or time-delayed ring cavity as analysed by Gibbs and coworkers[4].

The paper is organized in the following manner. Mathematical summary is provided in Sec. 2. An effort is made to avoid unnecessary mathematical and numerical details. Section 3 deals with the plane wave model using only the minimum of the symbolic dynamical methods needed for understanding of the bifurcation diagrams. In general, the mode of presentation is rather descriptive. Section 4 contains results on the transverse PCR with a fast Kerr-medium, and the last section is reserved for conclusions.

2. *Mathematical and numerical survey*

The PCR model adopted here assumes that the Kerr PCM is instantaneously responding, i. e. the cavity round-trip time is assumed to be much longer than the medium response time (MRT). It is also presumed that the potential instabilities in the intracavity field are not shorter than MRT. Under these conditions, as described in Ref. 10, the problem of solving wave equation can be reduced to iteration of an infinite dimensional map. The action of PCM is then represented by a nonlinear reflection, derived in Ref. 9:

$$E_b = iB_0 J_1(2|F_0 E_f^*|) \exp\left[i\,\mathrm{sgn}(n_2)(|F_0|^2 + |B_0|^2 + |E_f|^2)\right] \frac{\mathrm{sgn}(n_2) F_0 E_f^*}{|F_0 E_f^*|} \quad (1)$$

where $J_1(x)$ is the first-order Bessel function, and n_2 the second-order Kerr coefficient in the index of refraction. The fields are scaled by $1/\sqrt{n_2}$ times a factor which is different for the two models considered. In general, all the fields contained in Eq. (1) depend on the transverse coordinates x, y (and the time t), however, for numerical ease we confined our analysis to one transverse coordinate only. There is no reason to believe that inclusion of the other coordinate would alter our conclusions substantially. In addition, when the plane wave limit is considered, all transverse variations are neglected.

The overall propagation description of the PCR from Fig. 1, upon reflection, consists in free-space propagation to the aperture, filtering through the aperture, reflection from the normal mirror, and propagation back to the PCM, to close one complete round-trip:

$$E_f(x, t+\tau) = \exp(2ik_0 L)\,[FSP]\,[REFL] \exp\left(-\frac{x^2}{u^2}\right)[FSP]\,E_b(x, t). \quad (2)$$

Here τ is the dimensionless round-trip time, and $[FSP]$ stands for the free-space propagation, accomplished by the use of an FFT algorithm:

$$[FSP]\,E(x,t) = [FT]^{-1} \exp\left(-\frac{ik^2}{4\pi F}\frac{\tau}{2}\right)[FT]\,E(x,t), \tag{3}$$

where $[FT]$ and $[FT]^{-1}$ denote the Fourier transform and its inverse. $[REFL]$ is the normal mirror reflectilon operator,

$$[REFL] = r \exp\,(-2\pi\, iFLx^2/R). \tag{4}$$

r is the reflectivity of the mirror, $F = \frac{k_0 w_0^2}{2\pi L}$ is the resonators Fresnel number, u is the Gaussian aperture in units of w_0 and w_0 is the characteristic transverse spot-size which scales the transverse coordinate x. L and R are the length of the cavity and the radius of curvature of the normal mirror.

Eqs. (1) and (2) can be combined to a return map in the transverse coordinate:

$$E_f(t+\tau) = M\,[E_f(t)] \tag{5}$$

for each x. M is a nonlinear operator in the function space of fields E_f. For any initial time t Eq. (5) couples the field $E_f(t + n\tau) \equiv E_n$ to $E_f(t + n\tau + \tau) = E_{n+1}$. Our numerical procedure consists in repeated applications of the return map until a stable (or chaotic) mode distribution is reached. The intracavity field is probed at the PCM ($z = 0$) position, before reflection. The pump beams are assumed to be Gaussian of width w_0, $F_0(x) = B_0(x) = \sqrt{I_p}\exp(-x^2)$, or plane, for the plane wave case.

The treatment of the plane wave case differs in that Eq. (2) is simplified, since $[FSP] = 1$, $[REFL] = r$. Moreover, the optical pathlength $2k_0L$ is precisely that of axial rays, and the modes under consideration are axial. Actually, the analysis in the next section is done with $r = 1$ and for the wide open aperture, $u = \infty$.

3. *Plane wave approximation*

Some of the results on the plane wave approximation can be found in the second paper of Ref. 9. While that paper mostly deals with instabilities in the phase induced by period doubling, here we concentrate on the intensity period bifurcations, and performe a more complete analysis of the bifurcation diagram.

Thus looking at Eqs. (1) and (2) it is seen that the intracavity intensity $|E_n|^2 = I_n$ obeys a map relation:

$$I_{n+1} = |rB_0|^2\, J_1^2\,(2\sqrt{|F_0|^2\, I_n}), \tag{6}$$

which is reduced to a more convenient form:

$$x_{n+1} = A\, J_1^2 (\sqrt{x_n}) \tag{7}$$

by introducing the pump deriving parameter $A = |2rF_0B_0|^2$ and the intensity variable $x_n = 4|F_0|^2 I_n$. The dimensionless intensities are measured in units of $1/(k_0 d n_2)$, where d is the thickness of the medium. The mapping $J_1^2(\sqrt{x})$ function is depicted in Fig. 2. It is a multi-peaked function, whose maxima and minima are denoted by x_c^i on the graph. These points are collectively known as the critical points of the map.

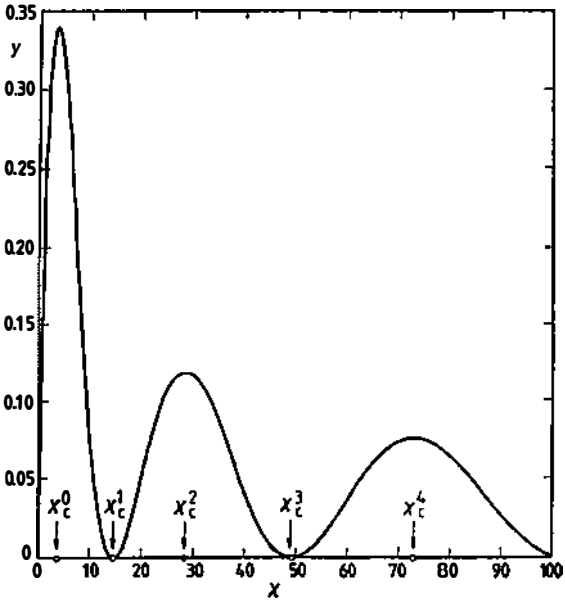

Fig. 2. The mapping function $y = J_1^2(\sqrt{x})$. It represents an example of a multimodal one-dimensional map. The x_c^i points: $x_c^0 \approx 3.38$, $x_c^1 \approx 14.7$, $x_c^2 \approx 28.4$, $x_c^3 \approx 49.2$, etc. are the critical points of the map. In the example considered in the text only the first two peaks of the function play the role.

In this manner, the initial wave equation for the forward and the backward waves is transferred into a discrete time-evolution equation. We are interested in the long-time behaviour of the system as the map (7) is iterated. What happens depends on the value of the driving parameter A. It is expected that for low values of A (more accurately up to $A_1 \approx x_c^1/J_1^2(\sqrt{x_c^0}) \approx 43.4$) the system follows Feigenbaum period doubling route, since the first part of the J_1^2 function resembles inverse parabola of the logistic map. This is what actually happens, as reported in Ref. 9. However, past the A_1 value the higher lobes of the Bessel function start to play the role, and the mapping seases to be unimodal. Its bifurcation diagram is shown in Fig. 3. It is seen that by increasing the pump driving, at a certain value the intracavity intensity becomes unstable, and starts to bifurcate following Feigen-

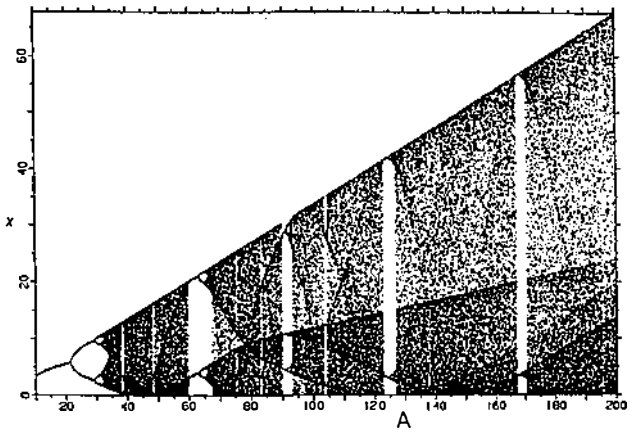

Fig. 3. Bifurcation diagram obtained by repeated interations of the one-dimensional map $x_{n+1} = AJ_1^2(\sqrt{x_n})$.

baum scenario. The initial P2 bifurcation corresponds to the excitation of half--axial modes, and it is of the same origin as the Ikeda instability in optical bistability. After the accumulation point has been reached, however, the bifurcation diagram loses any resemblence to the Feigenbaum. Nonetheless it still offers an interesting example of NL dynamical behaviour. Its global topological outlook can be explained, for example, by elementary symbolic dynamical methods[1,2]. Using these methods we show how to obtain the skeleton of the bifurcation diagram, i. e. the positions of the dark lines running through the diagram, and the positions and periodicity of various periodic windows seen in the chaotic region. This analysis is performed in the following manner.

As previously mentioned, the zeros and the maxima of the mapping function are known as the critical points x_c^l. These points are very special for the map, since they separate monotonic regions of the mapping function. When iterated, the system tends to wander longer around critical points. To start with, suppose that the input values of x_n are uniformly distributed, and that we are inside a chaotic region. After only one iteration the new x_{n+1} values will become nonuniform, clustered around the images of the critical points. Two of these images also define the extrema of the map, i. e. the boundaries of the output. After many iterations, it is clear that the images of the critical points will define a set of maxima in the distribution of x, which will show up in the bifurcation diagram as locations of the accumulation lines inside chaotic region. Accordingly, for each of the critical points a set of polynomials can be defined[1,2]:

$$P_0^l(A) = x_c^l, \tag{8a}$$

$$P_{n+1}^l(A) = A\,J_1^2\left[\sqrt{P_n^l(A)}\right]. \tag{8b}$$

These polynomials, when plotted as functions of A, determine locations of the dark lines embedded in a chaotic region. Few of the polynomials are drawn in Fig. 4. They say much about the dynamics of the system. As can be seen, most

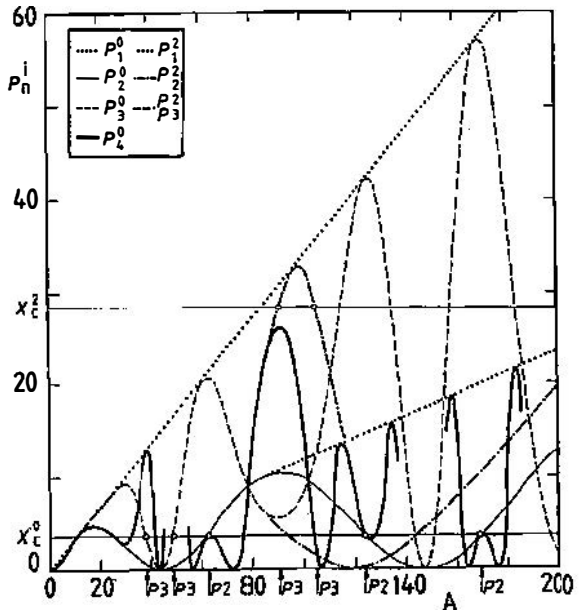

Fig. 4. $P_n^i(A)$ polynomials which explain the skeleton and the window structure of the bifurcation diagram from Fig. 3. Only the critical points x_c^0 and x_c^2 matter in the displayed region of the driving parameter A. Positions of the largest periodic windows and their periodicity are marked on the A axis.

of the features in the bifurcation diagram come from the first few critical points, most notably from x_c^0. For example, the upper boundary of the bifurcation diagram is determined by the first polynomial P_1^0 of x_c^0. The lower boundary, which is zero, comes from the first polynomial P_1^1 of the first zero x_c^1 of the Bessel function. Actually, all higher order polynomials of x_c^1 are also zero, and the same applies to all zeros of the mapping function. On the other hand, all straight lines seen in the diagram come from the first order polynomials of different maxima of the map.

The next important information about the transition scenario to be inferred from the symbolic analysis are the locations of the superstable n-orbits, around which periodic windows form in chaotic region. They are found among the real roots of the equations $P_n(A) = x_c$ for various i. This is also displaced in Fig. 4, where the location of the periodic orbits are marked on the A-axis at the intersections of various polynomials with the x_c^0 and x_c^2 horizontal lines. Perfect agreement is found.

Further, the chaotic band merging points can also be determined using P_n^i polynomials. For example, the $2 \to 1$ band-merging point seen at $A \approx 34$ is given as one of the roots of the equation $P_3^0(A) = P_4^0(A)$. The triple-merging point $P_2^0(A) = P_3^0(A) = P_4^0(A)$ seen at $A \approx 78$ is interesting because of the strong repulsion of the points between the bands in its vicinity. Such sudden changes in the attractor are indication of an interior crisis happening in the system.

While the intensity undergoes period doubling, the phase performes quasi-periodic hopping[9]: Lyapunov exponent of the phase evolution remains to be zero. Similar behaviour is observed in the full transverse model. There, even though

the intensity performes period doubling in the beginning, at high enough pump intensity the system evolves gradually towards high dimensional chaos. More and more Lyapunov exponents are becoming positive, and the attractors dimension is definitely larger than one, and increasing. However, the speed and the manner in which this infinitely dimensional system goes over to turbulent state decisively depends on the size of the aperture placed in the cavity.

4. *The transverse model*

In this section the full transverse case, Eqs. (1)—(2) is considered. The intensity of the pumps I_p is chosen as one of the control parameters, the other is the size of the Gaussian aperture u in front of the normal mirror. By changing the aperture size the behaviour of the system changes from one-dimensional like (for small apertures), to many-dimensional, with many degrees of freedom in which the system can grow. Other parameters in the problem (Fresnels number, radius of the mirror, etc.) are kept fixed.

We find that for the wide open aperture ($u = 8$) the transition to chaos is not a Feigenbaum period doubling as in the plane wave case, but a RTN scenario of few bifurcations of an invariant circle. By decreasing the aperture size we show how the transition changes from a RTN-like, with quickly establishing high dimensional chaos, to period doubling like, which change more gradually, and trend to develop strange looking windows.

We proceed numerically by adiabatically changing the pump intensity after each round trip. The typical increase ΔI_p (or decrease, if we consider down-sweeps) is of the order 10^{-5} (in units of the selfoscillation threshold intensity, which is the intensity unit here). Thus a typical bifurcation diagram is produced after 10^5 round trips. In this manner we try to avoid strong dynamical effects and spurious hysteresis[13]. Our criterion is that the up-sweep and the down-sweep should coincide. However, when there are coexisting attractors in the system (mode competition or optical bistability), hysteresis effects persist, and are unaffected by the slowdown in the sweep rate. Such instances are frequently observed in our model of PCR.

Even though the transverse dimension in included in the analysis, we show here only how the total intracavity intensity $I_f = \int_{-\infty}^{+\infty} dx\, |E_f(x)|^2$ changes as a function of the control parameters. The full transverse effects have been considered in detail elsewhere[10].

We start by displaying in Fig. 5 bifurcation diagrams for different aperture openings. They are seen to differ substantially. While in Fig. 5a there is an almost sudden change from a *P2* state to a featureless high dimensional attractor, in Fig. 5c and 5d clear Feigenbaum period doublings are observed, with interesting window structure. The transition in Fig. 5a represents an example of a RTN scenario. This is established by a closer inspection of the transition region using Poincare sections. At $I_p = 2.77$ the system is very close to a Hopf bifurcation. It spirals down to a pair of fixed points corresponding to the simple *P2* half axial mode. At $I_p = 2.775$ the limit cycle is well established, and at $I_p = 2.81$ it explodes, yielding to a different attractor. Such coexistence of attractors or mode compe-

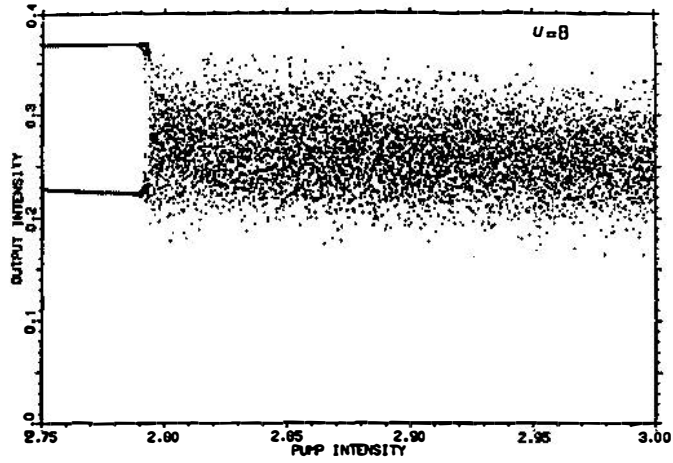
U=8
OUTPUT INTENSITY
0.0
0.1
0.2
0.3
0.4
2.75
2.80
2.85
2.90
2.95
3.00
PUMP INTENSITY

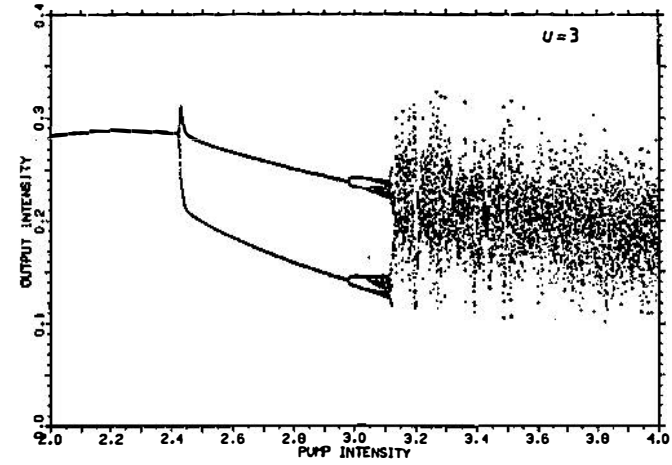
U=3
OUTPUT INTENSITY
0.0
0.1
0.2
0.3
0.4
2.0
2.2
2.4
2.6
2.8
3.0
3.2
3.4
3.6
3.8
4.0
PUMP INTENSITY

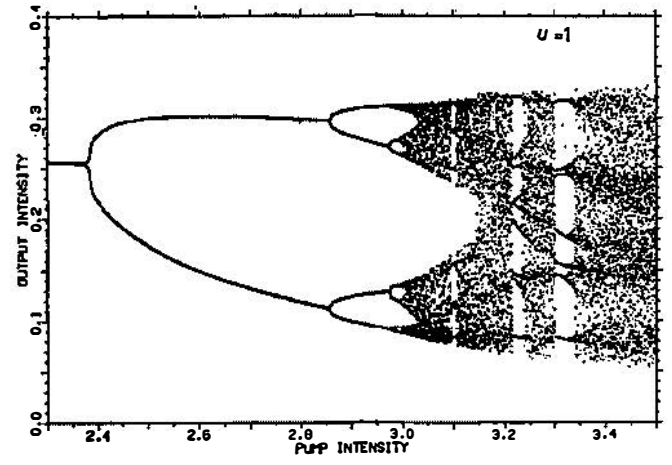
U=1
OUTPUT INTENSITY
0.0
0.1
0.2
0.3
0.4
2.4
2.6
2.8
3.0
3.2
3.4
PUMP INTENSITY

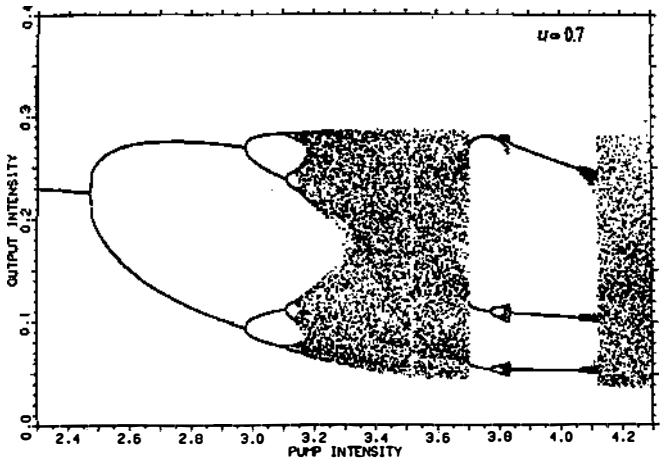

Fig. 5. Bifurcation diagrams of the transverse model as the size u of the Gaussian aperture is varied. The transition changes from the RTN scenario in (a) to a Feigenbaum-like period doubling in (d). While there are nine positive Lyapunov exponents in the case (a) as the chaos becomes *PI*-band, there is only one positive exponent in the cases (c) and (d).

tition is common in our system. The new limit cycle readily bifurcates at $I_p = 2.819$, then again at 2.8205, and finally at 2.8216. The last bifurcation is depicted in Fig. 6a. At $I_p = 2.82165$ a trace of frequency locking is observed, visible in Fig. 6b. Frequency locking is a sing of imminent transition to chaos, which actually happens at $I_p = 2.8217$, Fig. 6c. In this respect our system is very similar to fluid turbulent Reyleigh-Bernard flows with low aspect ratio[14], where similar quasiperiodic $\rightarrow$ $\rightarrow$ locked $\rightarrow$ chaotic sequence has been found. Past the value $I_p = 2.825$ high dimensional chaos is observed, with 9 positive Lyapunov exponents. Thus, opening of the aperture puts at the systems disposal many degrees of freedom, or many unstable directions in which to grow.

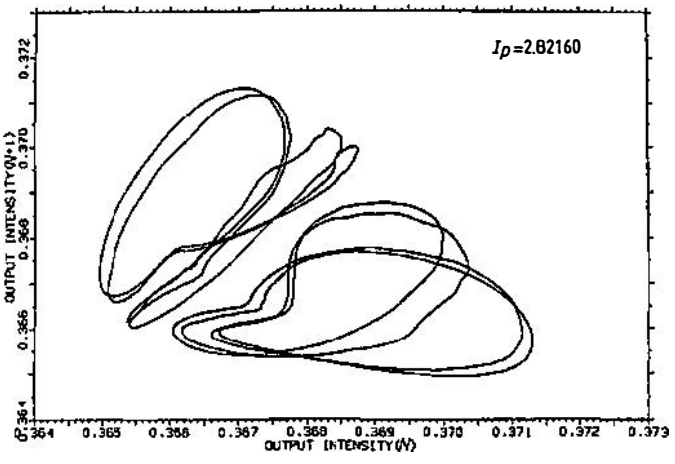

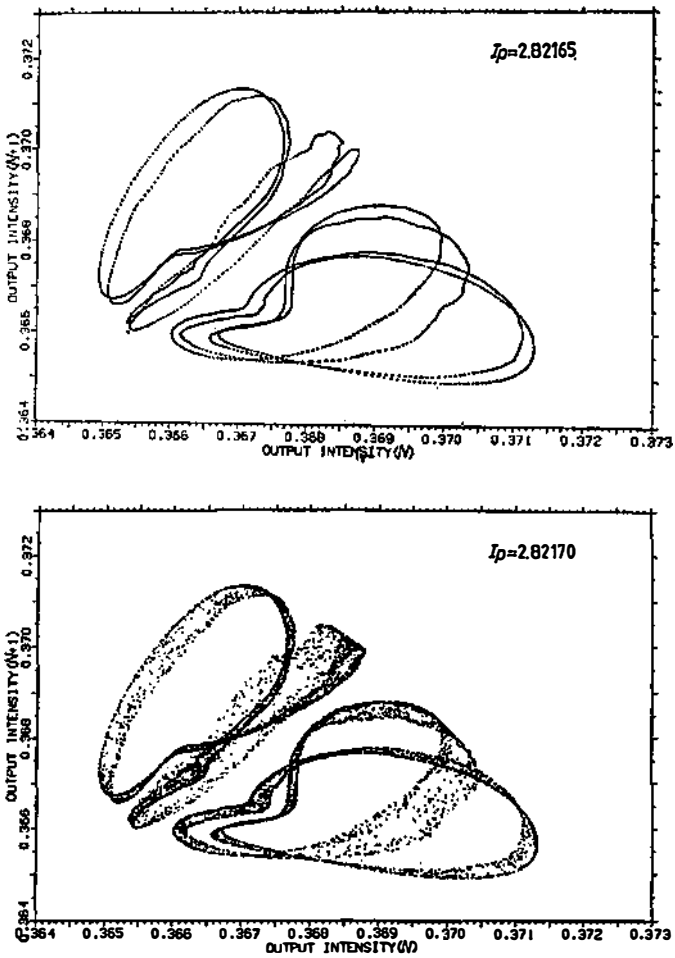

Fig. 6. Sudden transition to chaos from an invariant circle which bifurcated three times. The three plots are Poincare sections through the system from Fig. 5a. (a) represents the last bifurcation resolved, in (b) frequency locking at slightly increased pump intensity is noticed, and in (c) the system suddenly becomes chaotic. A great number of transients (of the order of 10^3) is killed before the plots are recorded.

On the contrary, reducing the aperture size constrains the system, and there is a tendency of developing along Feigenbaum-like scenarios. In this case central portions of the beam become more important, and the transverse variations lose in significance. For low intensity the system behaves more like one dimensional model. At high enough pump intensity, though, the system reaches featureless *P1* chaos. While for the case $u = 3$ this happens already at $I_p \approx 3.1$, for $u = 1$ the third Lyapunov exponent becomes positive only at $I_p \approx 4.2$.

The chaotic behaviour of the system at $u = 3$ is simple (Fig. 5b). In the beginning ($I_p \approx 3.2$—3.6) it oscillates between the *P2* and *P1* chaotic bands, later it stays as a *P1* chaos. No interesting periodic windows are observed. Much more

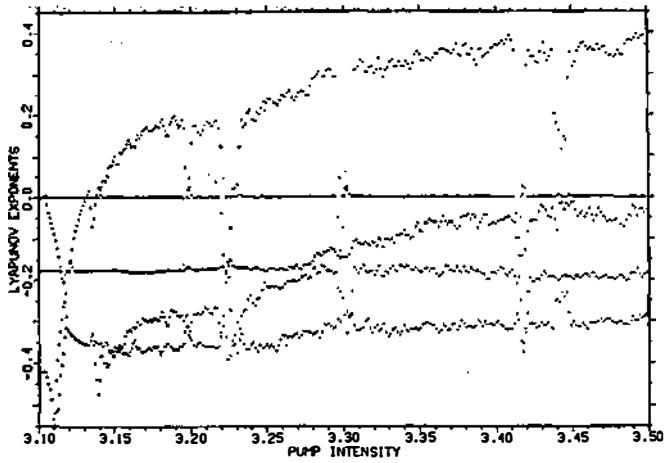

Fig. 7. The spectrum of Lyapunov exponents corresponding to the bifurcation diagram from Fig. 5c. The third Lyapunov exponent becomes positive at $I_p \approx 4.2$, so that the road to a high dimensional chaos is rather gradual.

interesting is the behaviour of the system for $u = 1$. Its Lyapunov spectrum is illustrated in Fig. 7. It follows well defined Feigenbaum route, with the first accumulation point at $I_p \approx 3.1$, when the second Lyapunov exponent becomes positive. The first one, describing indetermination of the phase, remains zero all the time. From the spectrum the Lyapunov dimension D_L can be found,

$$D_L = j + \frac{1}{|\lambda_{j+1}|} \sum_{i=1}^{i} \lambda_i \tag{9}$$

where $\lambda_1 > \lambda_2 > \ldots$ are the Lyapunov exponents, and j is the largest integer for which $\lambda_1 + \ldots + \lambda_j$ is still positive (or zero). Thus, below the accumulation point systems D_L dimension equals 1, at that point is jumps to 2, and then it grows (more rapidly in the beginning) to reach $D_L \approx 4.5$ at $I_p = 3.5$. This is to be contrasted, for example with the situation for $u = 8$, where already at $I_p = 2.825$ the D_L dimension approximately equals 18.6.

Various windows seen in Fig. 5c manifest themselves as dips in the positive Lyapunov exponent. The attractors fractal structure at $I_p = 3.16$ is depicted in Fig. 8. An intermittent chaotic 5-window is discovered at $I_p \approx 3.44$ (not resolved in Fig. 5c, but visible in the Lyapunov spectrum), and displayed in Fig. 9. This figure is recorded in the same manner as Fig. 5, only the sweep rate has been reduced. Upon reduction the intermittent chaotic nature of the window becomes more apparent: it breaks into a number of periodic regions separated by chaotic bursts.

By further reduction in the aperture size to the values of u less than one, the system has even less space to develop, and since it is dependent on more than one control parameter, the conditions for appearence of remerging period bifurcations are met[15]. Indeed such inverse bifurcations are visible in Fig. 5d around $I_p \approx 3.8$ in the broad *P3* window. Even more striking example of period »bubbling« is obser-

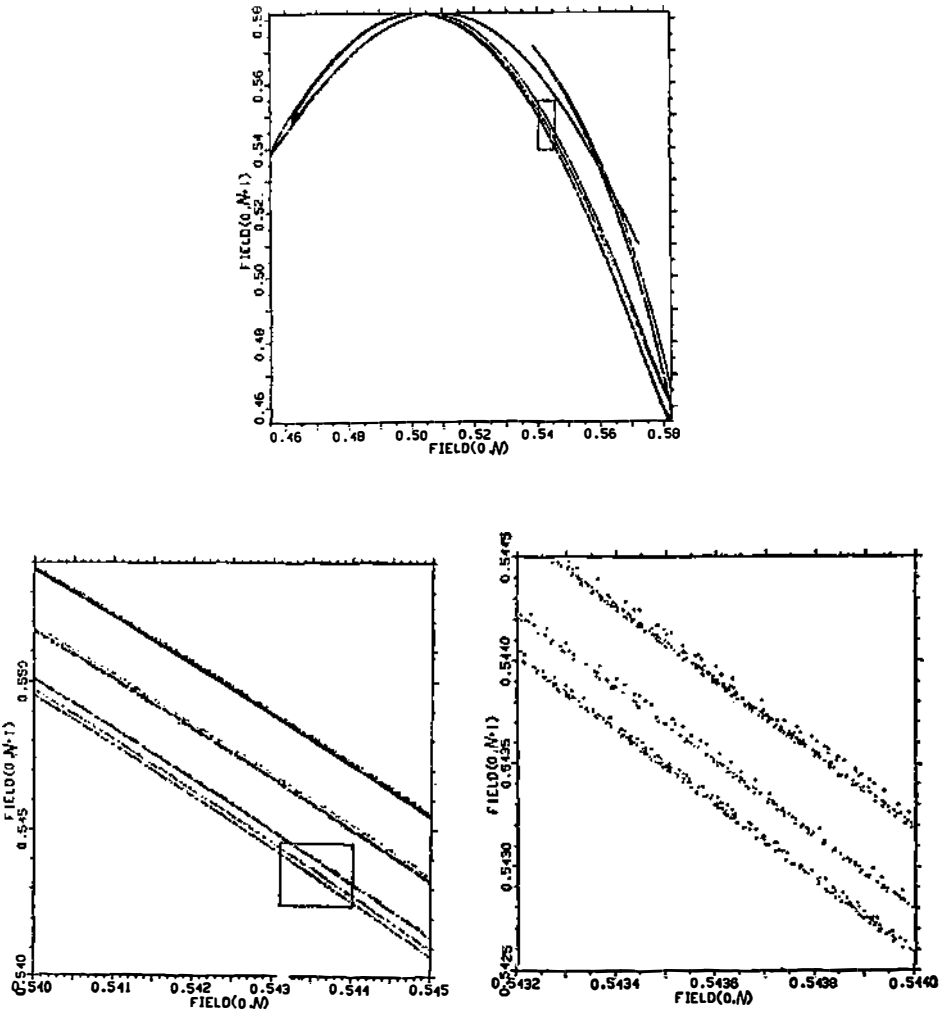

Fig. 8. Poincare section through the strange attractor form Fig. 5c at $I_p = 3.16$. The small inlet marked in (a) at a convenient place is enlarged in (b), and the small inlet in (b) is enlarged in (1). The approximate 3-2-1 local structure of lines (or sheets of the attractor) is seen to repeat itself on an ever smaller scale. Self-similar scaling, however, is not fully evident at this level of resolution.

ved if the systems development from Fig. 5d is followed further in intensity range (Fig. 10). At about $I_p \approx 4.4$ the system subduces to a gigantic *P4*, which at $I_p \approx 4.6$ develops periodic bubbles.

An important result of this analysis is that the metric entropy h, defined as the sum of the positive Lyapunov exponents, increases rather slowly with the dimension of the attractor. This means that the degree of chaoticity per dimension h/D_L is far lower than in the fully developed chaos of the plane wave model. The chaoticity decreases even further as the aperture is opened.

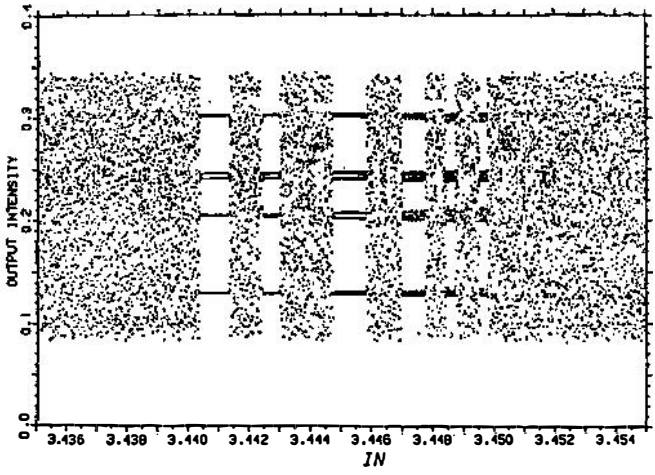

Fig. 9. Period 5 window at $I_p \approx 3.44$ from Fig. 5c. Upon reducing the sweep rate the $P5$ window breaks into intermittent chaos.

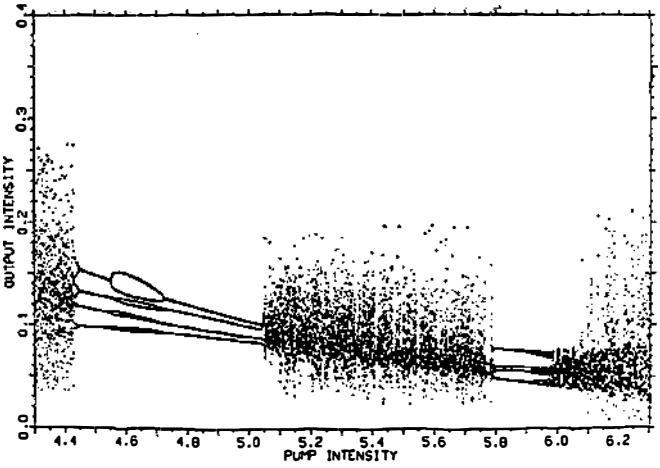

Fig. 10. Continuation of the Fig. 5d illustrating appearance of inverse bifurcations in the system for small aperture openings.

5. *Conclusions*

In this paper a transition to optical turbulence in a model of phase conjugate resonator has been investigated. Little is known about the transition to turbulence in infinitely dimensional systems. Farmer has considered the Mackey-Glass time--delay differential equation, which models blood production. Time delay serves as the variable which makes the system infinite, similar to the Ikeda model of passive ring cavity. Farmer found that the dimension of the MG attractor linearly

increases with the delay, while the entropy remains approximately the same. That means that Lyapunov exponents decrease with the driving, in contrast to our system. In our case metric entropy and the dimension of the attractor increase, but the rate of increase decreases as the pumps get stronger and the aperture gets wider. Thus, a chaotic attractor of a given dimension has more unstable directions in the MG system than in the PCR, but these are weakly chaotic in comparison to the fewer but more chaotic ones of the PCR. Though, the PCR system is becoming more similar to the MG as the aperture size is increased.

Similar conclusions to Farmers can be found in Ref. 4, where it was shown that there is no continuous limit between the short but finite medium response time, and the instantaneous response time for a plane wave approximation of Ikeda ring model. In essence, the authors[4] note that the routes to chaos are different for a 2D instantaneous and an ∞D time delay model, what is also found here. The results reported here, though, are for an instantaneous response time, but infinity is reached through transverse coupling by increasing the aperture size. In addition, we have performed calculations for short MRT[16] and found that in general they agree with the results reported here, provided there are no instabilities in the system which are shorter than the medium response time. Nonetheless, notable differences persisted in the dynamics, and the system preferred to go to chaos via a RTN scenario.

Finally, our results indicate that a more reliable and complete description of the dynamics and instabilities in PCR requires inclusion of the transverse effects. Dynamics which follow from a plane wave analysis, as exemplified by Fig. 3, and from an infinitely dimensional transverse model indeed differ considerably. In addition, in view of the results from Ref. 4, equally important seems to be inclusion of the finite time delay. However, considerable mathematical (numerical) difficulties in treatment of the complete model of PCR in space and time still preclude definitive conclusions.

Acknowledgement

One of the authors (MRB) acknowledges support from the Alexander von Humboldt Foundation.

References

1) J. V. Moloney, Phys. Rev. **33**A (1986) 4061; M. Le Berre, E. Ressayre, A. Tallet, K. Ta and H. M. Gibbs, IEEE J. Quantum Eletron. QE-**21** (1985) 1404;
2) For an introduction into phase conjugation and PCR-s see *Optical Phase Conjugation*, ed. by R. A. Fisher (Academic, New York, 1983);
3) A. Yariv, IEEE J. Quantum Electron, QE-**14** (1978) 650;
4) M. Le Berre, E. Ressayre, A. Tallet and H. M. Gibbs, Phys. Rev. Lett. **56** (1986) 274;
5) K. Ikeda, Opt. Commun. **30** (1979) 257; K. Ikeda, H. Daido and O. Akimoto, Phys. Rev. Lett. **45** (1980) 709;
6) As an introduction into chaos see H. G. Shusters, *Deterministic Chaos* (Physik Verlag, Berlin, 1985);
7) See *Optical Instabilities*, ed. by R. W. Boyd, M. G. Raymer and L. M. Narducci (Cambridge University Press, Cambridge, 1986); January Issue of J. Opt. Soc. Am. 2B (1985); J. Ackerhalt, P. W. Milonni and M. L. Shih, Phys. Rep. **128** (1985) 205;
8) This is also known as the thin-hologram regime, in which no Bragg conditions apply, and all diffraction orders are allowed;

9) E. M. Wright, P. Meystre and W. J. Firth, Opt. Commun. **51** (1984) 428; G. Reiner, P. Meystre and E. M. Wright, J. Opt. Soc. Am. **2B** (1985) 982;
10) G. Reiner, P. Meystre and E. M. Wright, to be published in J. Opt. Soc. Am.; J. Opt. Soc. Am. **4B** (1987) 865; G. Reiner, M. R. Belić and P. Meystre, to be published in J. Opt. Soc. Am.;
11) J. D. Farmer, Physica **4D** (1982) 366;
12) N. Metropolis, M. L. Stein and P. R. Stein, J. Combin. Theory **A15** (1973) 25; W. Z. Zheng, B. L. Hao, G. R. Wang and S. G. Chen, Commun. Theor. Phys. **3** (1984) 283; B. L. Hao, Lecture Notes for the Spring College in Nonlinear Physical Systems, 1986, ICTP Trieste;
13) R. Kapral and P. Mandel, Phys. Rev. **32A** (1985) 1076; For the kind of problems dynamical effects can cause, see the papers by D. M. Heffernan, Phys. Lett. **108A** (1985) 413; **109A** (1985) 465 and the comment on these papers by D. Dangoisse and P. Glorieux, Phys. Lett. **116A** (1986) 311;
14) H. L. Swinney, Physica **7D** (1983) 3;
15) M. Bier and T. C. Bountis, Phys. Lett. **104A** (1984) 239;
16) G. Reiner, PhD Thesis, Ludwig-Maximilians-Universität München (1987).

PRELAZ U OPTIČKU TURBULENCIJU KOD FAZNO-KONJUGOVANIH REZONATORA

MILIVOJ R. BELIĆ, G. REINER i P. MEYSTRE

Institut za fiziku, p. p. 57, 11001 Beograd

UDK 535.374

Originalni naučni rad

U radu su ispitivani mogući putevi u stanje optičke turbulencije kod fazno-konjugovanih rezonatora. Nelinearna dinamika modova unutar rezonatorske šupljine posmatrana je rešavanjem osne talasne jednačine uz korišćenje metoda brzog Fourier-ovog transforma i iterativnog preslikavanja. Jedna poprečna prostorna dimenzija je uključena u analizu, i više od jednog kontrolnog parametra je varirano tokom naših numeričkih ispitivanja. Utvrđeno je da putevi u haos kod ovog beskonačno-dimenzionog disipativnog sistema uključuju Feigenbaum-ovo udvostručenje periode, naizmenični haotično-periodični prelaz, kao i Ruelle-Takens-Newhouse-ov scenario. Registrovane su i druge zanimljive pojave, kao što su inverzne bifurkacije, tzv. unutrašnje krize atraktora, te koegzistirajući atraktori. Izvršeno je poređenje našeg beskonačno-dimenzionog optičkog sistema kako sa njegovom dvo-dimensionom aproksimacijom, tretiranom pomoću simboličkih dinamičkih metoda, tako i sa drugim beskonačnim sistemima, konkretno sa turbulentnim fluidima, te sa Mackey-Glass-ovim i Ikedinim modelima vremenskog kašnjenja.